Single-Particle Studies of Band Alignment Effects on Electron Transfer Dynamics from Semiconductor Hetero-nanostructures to Single-Walled Carbon Nanotubes

Chi-Tsu Yuan,[†] Yong-Gang Wang,[†] Kuo-Yen Huang,[†] Ting-Yu Chen,[†] Pyng Yu,[†] Jau Tang,[†,*] Amit Sitt,[‡] Uri Banin,[‡,*] and Oded Millo[§,*]

[†]Research Center for Applied Sciences, Academia Sinica, 128 Academia Road, Taipei 115-29, Taiwan, and [‡]Institute of Chemistry and [§]Racah Institute of Physics and the Center for Nanoscience and Nanotechnology, The Hebrew University, Jerusalem 91904, Israel

ABSTRACT

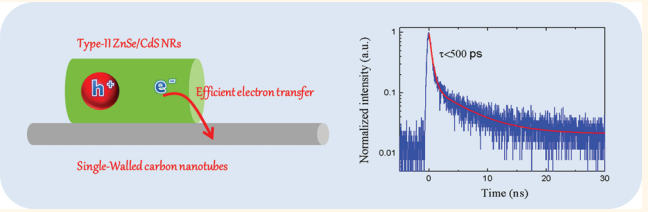

We utilize single-molecule spectroscopy combined with time-correlated single-photon counting to probe the electron transfer (ET) rates from various types of semiconductor hetero-nanocrystals, having either type-I or type-II band alignment, to single-walled carbon nanotubes. A significantly larger ET rate was observed for type-II ZnSe/CdS dot-in-rod nanostructures as compared to type-I spherical CdSe/ZnS core/shell quantum dots and to CdSe/CdS dot-in-rod structures. Furthermore, such rapid ET dynamics can compete with both Auger and radiative recombination processes, with significance for effective photovoltaic operation.

KEYWORDS: single-molecule spectroscopy · colloidal nanocrystals · carbon nanotubes

Inorganic colloidal semiconductor quantum dots (QDs) exhibit unique optical properties, including large absorption cross sections, broad absorption bands, tunable band gap by control of size and shape, high photo- and chemical stability, possibility for multiple exciton generation, and hot-electron transfer.[1−3] These properties are beneficial to photovoltaic (PV) operation, and consequently, they are being investigated for use as sensitizers for light-harvesting applications.[4,5] In addition, colloidal QDs share all of the main advantages of conventional organic dyes, for example, low-cost fabrication, solution processing, and well-controlled synthesis methods. Therefore, colloidal QDs show potential for integration in future generations of solar cell devices. Unfortunately, low efficiencies were reported so far for QD-based PV devices, and this is commonly attributed mainly to low electron-injection rates as compared to other competing processes, including radiative and nonradiative recombination.[6] Obviously, further investigation is required in order to gain better understanding of the above fundamental issues, which may improve the performance of QD-based PV and other optoelectronic devices.

The utilization of colloidal QDs in optoelectronics was restricted also by poor transport properties owing to their insulating surface. For PV operation, the photogenerated excitons need to be dissociated into free charge carriers, then extracted and redirected to respective electrodes. Unlike p−n junction-type solar cells, no built-in electric fields can be exploited to separate electron−hole pairs. In addition, direct charge transport among QDs is difficult. Therefore, additional materials serving as electron acceptors and conductors need to be introduced along with the QDs to form PV devices.[1,7]

Single-walled carbon nanotubes (SWCNTs) that have a high aspect ratio and large surface area can accommodate a large amount of sensitizers and at the same time provide direct electrical pathways for charge-carrier transport owing to their one-dimensional nature.[8] CNTs have high electron affinity and exhibit excellent electrical properties, including high electron mobility,

* Address correspondence to jautang@gate.sinica.edu.tw, banin@chem.ch.huji.ac.il, milode@vms.huji.ac.il.

Received for review August 21, 2011 and accepted November 29, 2011.

Published online December 02, 2011
10.1021/nn2036957

that can provide ballistic conduction pathways.[9] Indeed, it has been shown that SW-CNTs can play important roles in PV operation, functioning as electron acceptors as well as conductors.[10,11] Therefore, the integration of colloidal QDs with SW-CNTs can be utilized as a potential architecture for future PV applications by taking advantages of the unique properties of both constituents.[12−14]

So far, the studies of the interactions between colloidal QDs and SW-CNTs focused mainly on ensembles of core-only CdSe or type-I core/shell CdSe/ZnS QDs and CNTs.[15−17] However, such conventional ensemble measurements could only provide average information while masking important unique single-particle behaviors. In addition, inherent heterogeneity of sizes, shape, and local environments within the same batch would affect the charge transfer dynamics, partly due to competing Förster-type energy transfer between neighboring QDs of different sizes. The single-molecule spectroscopy (SMS) technique provides a powerful tool to investigate complex interactions down to the single-QD level. Recently, such SMS has been successfully applied in studies of charge transfer dynamics from colloidal QDs to various charge acceptors, including TiO_2 and C_{60}.[18,19]

According to the Marcus theory, the electron transfer (ET) rate between single donor−acceptor states, k_{ET} can be described by

$$k_{ET} = \frac{2\pi}{\hbar}|H_{DA}|^2 \frac{1}{\sqrt{4\pi\lambda k_B T}} \exp[-(\lambda+\Delta G^0)^2/4\lambda k_B T] \quad (1)$$

where H_{DA}, ΔG^0, λ, and T are the electronic coupling strength between the initial and final states, the Gibbs free-energy difference between the donor and acceptor states (driving force), the reorganization energy, and the temperature, respectively.[20] Therefore, three factors can be adjusted to control the ET rates at a fixed temperature. Most of the previous reports have concentrated on the influence of the reorganization energy or driving force on the ET rates between colloidal QDs and TiO_2 nanoparticles, by changing the solution dielectric properties or QDs' sizes.[21−23] In contrast, in the case of electron transfer from colloidal QDs to SW-CNTs, the driving force is much larger than the reorganization energy ($-\Delta G_0 > \lambda$), and then the ET rate could be controlled by the pre-exponential term of eq 1, mainly by the electronic coupling strength.[24,25] Evidence for that is provided by a previous report in which it was demonstrated that, by integrating CdTe/CdSe type-II QDs with molecular acceptor (anthraquinone), ultrafast charge separation and slow recombination can be achieved, as monitored by ensemble ultrafast spectroscopy.[26]

In this work, the effect of the electronic coupling on ET rates was investigated by combining time-correlated single-photon counting and single-molecule spectroscopy. A key point is our demonstration that the ET rates can be modified dramatically for hybrid semiconductor nanostructures consisting of a QD within a NR with type-II band alignment (ZnSe seeded CdS NRs) relative to heterostructures having type-I band alignment (spherical CdSe/ZnS QDs or CdSe seeded CdS NRs). Importantly, the ET rate observed for the type-II ZnSe/CdS QD/NR system is larger than those of both the nonradiative Auger process and the radiative recombination.

RESULTS AND DISCUSSION

The ET rate is expected to decay exponentially with increasing separation between the electron donor and acceptor materials and can be expressed as $k_{ET} = k^0_{ET}\exp(-\beta d)$, where k^0_{ET}, β, and d are the intrinsic ET rate, attenuation factor, and separation between donor and acceptor, respectively. In order to explore the intrinsic ET process, dilute QD (or QD/NR) solutions were deposited on highly dense (>95% surface coverage) SW-CNT-coated substrate by spin-coating or drop-casting, as shown in Figure S1a (Supporting Information).[15] The colloidal nanostructures thus adhered physically to the SW-CNTs *via* the van der Waals force without a chemical linker. Such a chemical linker is expected to reduce the ET rate owing to the increase in QD−CNT distance beyond that determined by the length of the capping organic ligands [triocyl phosphine oxide (TOPO)]. Moreover, linker molecules may also disturb the intrinsic QD properties. In order to demonstrate the QD adsorption, we present in Figure S1b an atomic force microscopy topographic image measured, for clarity, on CdSe/ZnS core/shell QDs deposited on a low-concentration SW-CNT-coated substrate, where a height profile taken along the green dotted line is presented in panel c. The height determined from this profile, ~12 nm, is consistent with the sum of the SW-CNTs' (~2 nm) and QDs' (~8 nm) diameters, in particular when taking into consideration the effect of the capping ligands. Obviously, not all of the QDs adsorb in a way to form strong coupling of the CNTs, and some fraction of them only weakly interact with CNTs. Fortunately, these latter QDs can be readily identified by checking their fluorescence properties, as detailed below.

To estimate the interfacial ET rates, time-resolved fluorescence measurements were performed on nanocrystals that were either close to or well-separated from the CNTs. The measured lifetime should obviously decrease (for any type of colloidal nanostructure studied here) upon introducing the additional nonradiative channel of ET to the CNT. Thus, we can derive the interfacial ET rates by a simple expression, $k_{ET} = 1/\tau_{QD-CNT} - 1/\tau_{QD}$, where the first term corresponds to the lifetime measured for a QD near the CNT and the second term for an isolated QD. Obviously, this is only an approximation since energy transfer processes may also be involved, depending on the strength of the QD−CNT interaction. We will show below, however,

how one can single out those nanocrystals in which the charge transfer process dominates. Due to inevitable sample heterogeneity, in particular, variations in the degree of QD−CNT coupling, we randomly measured tens of QDs of each type, enabling us to construct a reliable statistical distribution.

We first present and address our measured results for CdSe/ZnS core/shell QDs with type-I band alignment. Figure 1 shows the fluorescence lifetime imaging for single colloidal QDs adsorbed on SW-CNTs (a) and on glass coverslip (b) as reference. Indeed, the difference between the fluorescence lifetimes of these two samples is quite noticeable, being much shorter for the QDs adsorbed on the CNTs. To gain more insight into fluorescence variations, single-QD fluorescence was measured for more than 40 individual QDs adsorbed onto SW-CNTs, showing that the lifetimes of QDs attached to SW-CNTs ranged mainly between 4 and 8 ns, yet still involving a few QDs with significantly longer lifetimes, likely due to weak interaction with CNTs. In contrast, the peak of the lifetime distribution histogram is centered at ~20 ns for isolated QDs without coupling to CNTs (see Supporting Information, Figure S2).

Typical fluorescence time trajectories of single QDs deposited on SW-CNTs are displayed in Figure 2a,b. Qualitatively, two groups of QDs exhibiting distinct fluorescence time trajectories were found, either preserving the ordinary on−off blinking behavior (26 QDs, Figure 2a) or showing relatively continuous emission without long-lived dark periods (14 QDs, Figure 2b). We attribute these two very different behaviors to the situations of a QD coupled, respectively, to either semiconducting or metallic SW-CNTs (known to naturally coexist within a batch). Previous reports have demonstrated that fluorescence intermittency (blinking) can be suppressed significantly by introducing an efficient energy transfer process when QDs are placed in proximity to metallic surfaces, metallic nanostructures, and graphene sheets.[27−30] In this case, the exciton energy can be transferred efficiently to metallic materials, leading to annihilation of electrons and holes simultaneously. Upon such energy transfer, the QD would remain at a neutral bright state, thus competing with the formation of the charged dark state. As a result, reduced blinking accompanied with quenched fluorescence intensity was observed, which is consistent with our experimental results presented in Figure 2b. This energy transfer process typically resulted also in reduced lifetime, as shown in Figure S3.

In contrast, pure electron transfer processes should still manifest on−off blinking but with shorter on-time durations compared to the case of isolated QDs.[18] This is because the additional charge transfer route enhances the ejection rate of electrons from the QD, resulting in positively charged QDs and thus entering the dark state more frequently. Such a behavior is depicted in Figure 2a. Obviously, the effects of charge transfer on blinking can be more intricate than this simple consideration. It may also depend on which kinds of charges (electrons or holes) are injected and the influence of backward electron transfer. Nevertheless, we can use the effect portrayed in Figure 2 in order to select (and then study) those nanocrystals in which ET is the dominant process enhancing the fluorescence decay rate. Namely, by prechecking the fluorescence time traces, we can find the suitable QDs (exhibiting blinking) for our studies of charge transfer dynamics.

To determine the ET rates, time-resolved fluorescence measurements were performed for single colloidal CdSe/ZnS QDs (with type-I band alignment) deposited on a SW-CNT-coated glass substrate and on a bare glass coverslip for reference. Obviously, the measured fluorescence lifetime was found to be faster for QDs on SW-CNTs as compared to the reference (regardless of the blinking behavior). Tens of QDs were measured in our experiments, and two representative ones (that exhibited blinking), accompanied with a reference QD (on glass), are shown in Figure 3. The derived ET rates (on CNTs) were distributed in the range of 5×10^7 to 1.5×10^8 s^{-1}. This distribution of ET rates obtained by SMS is a typical phenomenon, owing to sample heterogeneity, including variations in SW-CNT chirality, QD shell thickness, and the QD−CNT distance and coupling.[31]

This injection rate from the type-I CdSe/ZnS QDs to SW-CNTs is comparable to that of the radiative recombination and is still far smaller than the Auger recombination rate.[32] The ET rate is restricted by the strong confinement of the electron ground state wave function within the core by the shell barrier. Further enhancement of the ET rate is obviously desirable for realization of high-performance QD-based solar cells. Additionally, bare core QDs may suffer from photoinduced oxidation, also limiting their utility as light sensitizers. On the basis of the Marcus theory, for the case of the ET process from CdSe QDs to TiO_2, the ET rate can be increased significantly by increasing the driving force through reducing QD sizes thanks to the quantum confinement effect (Marcus normal regime). In light of Marcus theory, an alternative to accelerate ET rate is to enhance the electronic coupling strength between the donor and acceptor states, and this is the strategy we used here.

Following the above considerations, we replaced the (more common) type-I CdSe/ZnS core/shell QDs with seeded ZnSe/CdS QD/NR nanocrystals that have an internal staggered, type-II band alignment.[33] To keep the same driving force, special care was taken to have the emission wavelength of the type-II QDs/NRs close to that of type-I core/shell QDs. In such type-II configuration, the electrons are delocalized over the 1-D NRs, whereas the holes are confined within the QD core, leading to an increase of the electronic coupling to neighboring acceptor states supported by the SW-CNTs, along with decreasing electron/hole wave function overlap. As a result, the radiative lifetime of

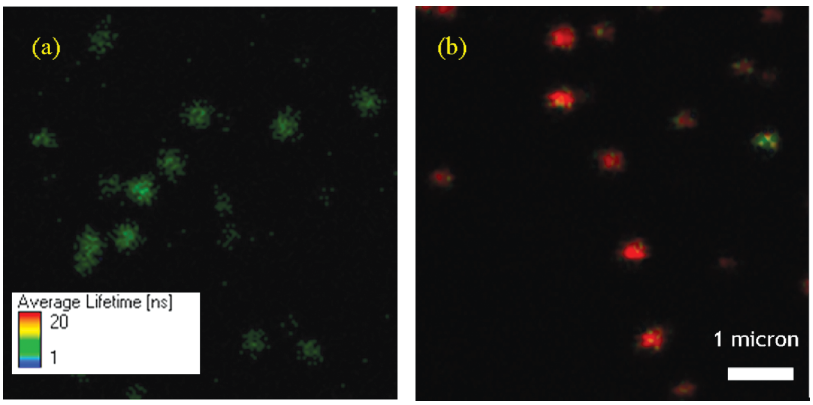

Figure 1. Fluorescence lifetime imaging (FLIM) of colloidal CdSe/ZnS QDs deposited on SW-CNTs (a) and on bare glass coverslip (b). Evidently, the lifetimes are shorter for QDs deposited on the SW-CNTs.

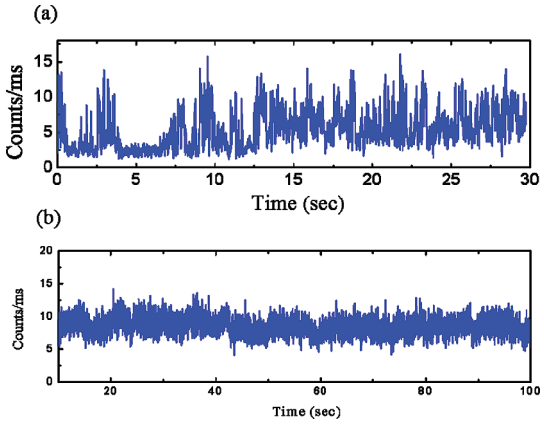

Figure 2. Fluorescence time trajectories of single CdSe/ZnS QDs deposited on SW-CNT-coated substrates. Trace (a) shows blinking and is attributed to a QD positioned near a semiconducting CNT, while (b) corresponds to a QD near a metallic one.

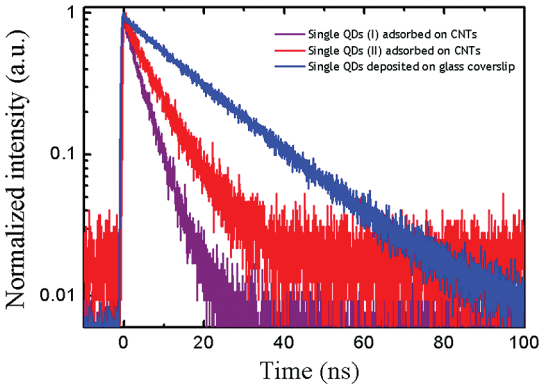

Figure 3. Two fluorescence decay profiles of single CdSe/ZnS QDs deposited on SW-CNT-coated glass substrates. For comparison, a measurement acquired for a QD deposited on bare glass, showing the slower decay, is also displayed.

the corresponding type-II exciton is typically longer than those of its type-I counterpart. Moreover, unwanted Auger recombination can also be mitigated, leading to better charge separation and extraction.[34,35]

To demonstrate the unique properties of type-II QD/NR systems, a representative (out of 33 measured nanoparticles) fluorescence decay profile for a single rod excited under single-exciton regime is displayed in Figure 4. The average number of photogenerated excitons can be estimated by $N_{excitons} = I\sigma/h\upsilon$, where I, σ, and $h\upsilon$ are the excitation intensity, absorption cross section, and excitation photon energy, respectively. This decay can be fitted well by a biexponential decay curve with one long lifetime component of ~78 ns and a short lifetime component of ~3.5 ns (see Supporting Information). The long component is assigned to the radiative decay lifetime of the type-II excitons, while the short lifetime is attributed to Auger recombination of the charged excitons. In a previous report, it was demonstrated that the Auger lifetime can be lengthened up to ~10 ns for quasi-type-II CdSe QDs with thick CdS shells.[35,36] As compared with the conventional type-I QDs, the radiative decay rates of type-II excitons can be reduced by a factor of ~4 along with the suppression of the Auger process by more than 1 order of magnitude. Consequently, such type-II heterostructures possess two inherent advantages for charge separation and extraction.

We also performed time-resolved fluorescence measurements to determine the ET rates from type-II QDs/NRs to SW-CNTs, as shown in Figure 5a. For a fraction of such nanocrystals studied (see distribution presented in Figure S4 of the Supporting Information), the fluorescence decay is dominated by an initially fast decay component (>85% contribution) with a lifetime ranging between 500 ps and 1 ns, which is comparable to the instrumental response function of our detection system. Such a fast decay was not observed for the isolated QD/NRs not coupled to SW-CNTs and is attributed to the contribution of a new additional nonradiative process induced by SW-CNTs, thus most likely electron transfer from the type-II seeded NRs to the SW-CNT, as shown in Figure 5b. Due to the electron delocalization over the CdS NRs, the electronic coupling strength between the donor and acceptor states can be enhanced significantly to facilitate the ET process. The charge injection rate is estimated to be about ~10^9 Hz, which makes it more efficient than the Auger process and much faster than the

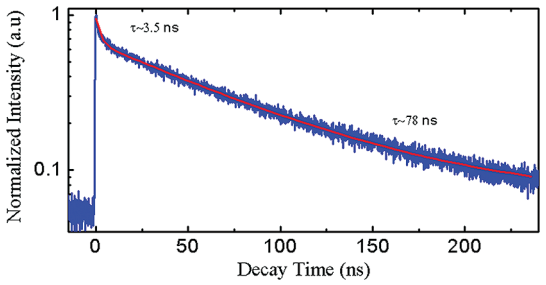

Figure 4. Fluorescence decay profile of a single ZnSe/CdS QD/NR with type-II band alignment.

radiative recombination. In addition, such an electron injection rate is also faster than that of the previously studied type-I CdSe/ZnS QDs to TiO_2 nanoparticles.[18] Hence, it provides an opportunity to further improve the PV performance of QD-based solar cells.

To optimize the extraction of the photogenerated electrons, the ET rates must prevail over all other competing pathways, mainly including radiative and Auger recombination. For comparison, we defined a factor to quantify the ET process, $F = \log(k_{ET}^2/(k_{Radiative} \times k_{Auger}))$, which involves the contributions of the radiative and Auger recombination. For $F = 0$, the charge injection rate is comparable to all other competing processes. In the case of type-II NRs, this F value is at least larger than 2, indicating that such charge transfer is the dominant process.

Finally, in order to check whether it is indeed the different type of band alignment or possibly the different nanocrystal geometry that brings about the different behaviors reported above, we also measured the ET rates from CdSe/CdS QDs/NRs to SW-CNTs. These nanocrystals have a similar shape to the above ZnSe/CdS heterostructures, but possess type-I band alignment (although rather marginally).[37] First we note that the fluorescence lifetime of CdSe/CdS QDs/NRs on bare glass was found to be ~13 ns, which is consistent with a previous report.[38] Figure S5 shows the fluorescence decay profiles of a single CdSe/CdS QD/NR adsorbed on a SW-CNT assembly deposited on a glass substrate. The observed ET rate, determined by averaging over 31 particles for this system, was found to be $\sim 1 \times 10^8\ s^{-1}$ (see Supporting Information) comparable to that of the type-I CdSe/ZnS core/shell QDs (and much smaller compared with the type-II QD/NR structure). It is thus reasonable to assume that in both type-I heterostructures studied here, irrespective of geometry, the electrons were injected directly from the CdSe core to the SW-CNTs through the shell barrier. Indeed, upon drop-casting, the QD/NR nanocrystals lie

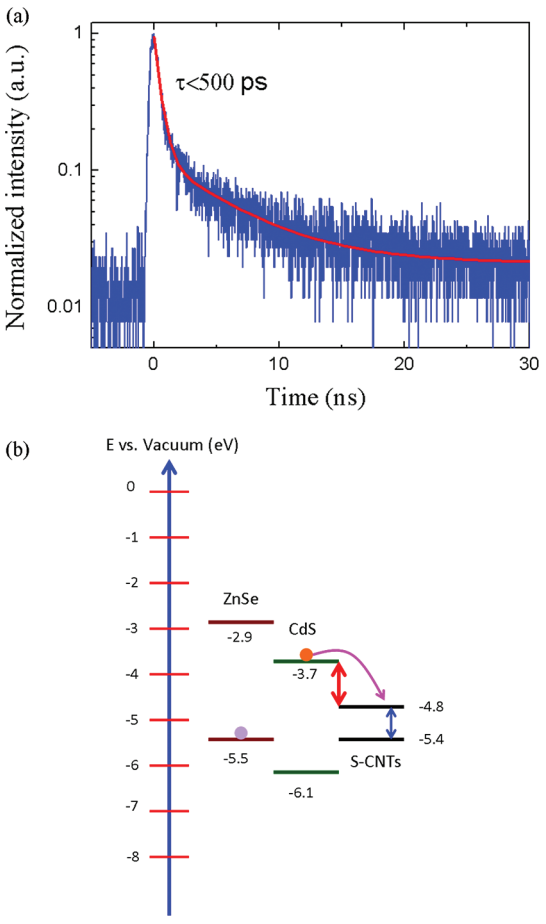

Figure 5. (a) Fluorescence decay profiles of a single seeded ZnSe/CdS QD/NR deposited on SW-CNT-coated substrate. (b) Scheme of the relative energy level positions in the CNT−hetero-nanorod composite system investigated here.

flat on top of the SW-CNTs. Thus, the electrons within the embedded QD would transfer to the SW-CNTs through a thin shell barrier of the side walls, leading to ET rates similar to those observed for the spherical core/shell heterostructures.

CONCLUSIONS

In summary, time-resolved fluorescence measurements on single nanocrystals of various types clearly indicate that the electron transfer to nearby single-walled carbon nanotubes is most effective for dot-in-rod heterostructures with type-II band alignment. In particular, in the case of ZnSe/CdS QD/NR nanostructures, the ET dynamics was found to prevail over both Auger and radiative recombination processes, making composites consisting of such particles and CNTs promising candidates for photovoltaic applications.

EXPERIMENTAL SECTION

For single-particle measurements, extremely dilute colloidal solution (about nanomolar concentration) was dispersed onto the glass substrate coated with or without SW-CNTs. A pulsed diode laser with a wavelength of ~460 nm as an excitation source was focused onto the sample by a microscope objective. The fluorescence was collected by the same objective and guided to a confocal pinhole (~50 μm) to reject out-of-focus light.

After the pinhole, the fluorescence was filtered by a suitable band-pass filter and finally detected by a single-photon avalanche photon diode (APD, MT 200, PicoQuant). TTL pulses from an APD are fed into a time correlator (PicoQuant, PH 300) to calculate TCSPC histograms. To perform photon correlation measurement, the fluorescence beam was further split into two beams *via* a 50/50 nonpolarizing beam splitter cube and detected by a pair of avalanche photodiodes. The intensity autocorrelation function can be obtained by SymPhoTime software (PicoQuant). As shown in Figure S7, a typical photon antibunching behavior can be observed, which is a hallmark of single-QD emission, thus enabling us to confirm that the emission is indeed from single QDs.

ZnSe/CdS and CdSe/CdS QD/NR heterostructures were synthesized by seeded growth methods following the work of refs 33 and 37. Single-walled carbon nanotubes were deposited on the substrate by a self-assembly process according to ref 39.

Acknowledgment. This research was supported by grants from Academia Sinica (J.T., U.B., O.M.) NSC of Taiwan (J.T.), the ERC project DCENSY (U.B.), and by the Israel Science Foundation (O.M.). O.M. acknowledges support from the Harry de Jur Chair in Applied Science. U.B. thanks the Alfred and Erica Larisch Memorial Chair.

Supporting Information Available: Additional figures and experimental details. This material is available free of charge *via* the Internet at http://pubs.acs.org.

REFERENCES AND NOTES

1. Kamat, P. V.; Tvrdy, K.; Baker, D. R.; Radich, J. G. Beyond Photovoltaics: Semiconductor Nanostructures for Liquid-Junction Solar Cells. *Chem. Rev.* **2010**, *110*, 6664–6688.
2. Tisdale, W. A.; Williams, K. J.; Timp, B. A.; Norris, D. J.; Aydil, E. S.; Zhu, X. Y. Hot-Electron Transfer form Semiconductor Nanocrystals. *Science* **2010**, *328*, 1543–1547.
3. McGuire, J. A; Sykora, M.; Joo, J.; Pietryga, J. M.; Klimov, V. I. Apparent *versus* True Carrier Multiplication Yields in Semiconductor Nanocrystals. *Nano Lett.* **2010**, *10*, 2049–2057.
4. Gur, I.; Fromer, N. A.; Geier, M. L.; Alivisatos, A. P. Air-Stable All-Inorganic Nanocrystal Solar Cells Processed from Solution. *Science* **2005**, *310*, 462–465.
5. Salant, A.; Shalom, M.; Hod, I.; Faust, A.; Zaban, A.; Banin, U. Quantum Dot Sensitized Solar Cells with Improved Efficiency Prepared Using Electrophoretic Deposition. *ACS Nano* **2010**, *4*, 5962–5968.
6. Hodes, G. Comparison of Dye- and Semiconductor-Sensitized Porous Nanocrystalline Liquid Junction Solar Cells. *J. Phys. Chem. C* **2008**, *112*, 17778–17787.
7. Barea, E. M.; Shalom, M.; Gimenez, S.; Hod, I.; Mora-Sero, I.; Zeban, A.; Bisquert, J. Design of Injection and Recombination in Quantum Dot Sensitized Solar Cells. *J. Am. Chem. Soc.* **2010**, *132*, 6834–6839.
8. Yu, K.; Chen, J. H. Enhancing Solar Cell Efficiencies through 1-D Nanostructures. *Nanoscale Res. Lett.* **2009**, *4*, 1–10.
9. Dillon, A. C. Carbon Nanotubes for Photoconversion and Electrical Energy Storage. *Chem. Rev.* **2010**, *110*, 6856–6872.
10. Weaver, J. E.; Dasari, M. R.; Datar, A.; Talapatra, S.; Kohli, P. Investigating Photoinduced Charge Transfer in Carbon Nanotube–Perylene–Quantum Dot Hybrid Nanocomposites. *ACS Nano* **2010**, *4*, 6883–6893.
11. Hu, L. G.; Zhao, Y. L.; Ryu, C. G.; Stoddart, J. F. Light-Induced Charge Transfer in Pyrene/CdSe-SWNT Hybrids. *Adv. Mater.* **2008**, *20*, 939–946.
12. Shukla, S; Ohulchanskyy, T. Y.; Sahoo, Y.; Samoc, M.; Thapa, R.; Cartwright, A. N.; Prasad, P. N. Polymeric Nanocomposites Involving a Physical Blend of IR Sensitive Quantum Dots and Carbon Nanotubes for Photodetection. *J. Phys. Chem. C* **2010**, *114*, 3180–3184.
13. Cho, N.; Choudhury, K. R.; Thapa, R. B.; Sahoo, Y.; Ohulchanskyy, T.; Cartwright, A. N.; Lee, K. S.; Prasad, P. N. Efficient Photodetection at IR Wavelengths by Incorporation of PbSe–Carbon-Nanotube Conjugates in a Polymeric Nanocomposite. *Adv. Mater.* **2007**, *19*, 232–236.
14. Schulz-Drost, C.; Saobba, V.; Gerhards, C.; Leubner, S.; Krick Calderon, R.; Ruland, A.; Guldi, D. M. Innovative Inorganic–Organic Nanohybrid Materials: Coupling Quantum Dots to Carbon Nanotubes. *Angew. Chem., Int. Ed.* **2010**, *49*, 6425–6429.
15. Jeong, S.; Shim, H. C.; Kim., S.; Han, C. S. Efficient Electron Transfer in Functional Assemblies of Pyridine-Modified NQDs on SWNTs. *ACS Nano* **2009**, *4*, 324.
16. Crooker, S. A.; Hollingsworth, J. A.; Tretiak, S.; Klimov, V. I. Spectrally Resolved Dynamics of Energy Transfer in Quantum-Dot Assemblies: Towards Engineered Energy Flows in Artificial Materials. *Phys. Rev. Lett.* **2002**, *89*, 186802.
17. Juarez, B. H.; Meyns, M.; Chanaewa, A.; Cai, Y.; Klinke, C.; Weller, H. Carbon Supported CdSe Nanocrystals. *J. Am. Chem. Soc.* **2008**, *130*, 15282–15284.
18. Jin, S.; Lian, T. Electron Transfer Dynamics from Single CdSe/ZnS Quantum Dots to TiO_2 Nanoparticles. *Nano Lett.* **2009**, *9*, 2448–2454.
19. Song, N.; Zhu, H.; Jin, S.; Zhan, W.; Lian, T. Poisson-Distributed Electron-Transfer Dynamics from Single Quantum Dots to C60 Molecules. *ACS Nano* **2011**, *5*, 613–621.
20. Marcus, R. A. On the Theory of Oxidation–Reduction Reactions Involving Electron Transfer. I. *J. Chem. Phys.* **1956**, *24*, 966–978.
21. Hyun, B. R.; Bartnik, A. C.; Lee, J. K.; Imoto, H.; Sun, L. G.; Choi, J. J.; Chujo, Y.; Hanrath, T.; Ober, C. K.; Wise, F. W. Role of Solvent Dielectric Properties on Charge Transfer from PbS Nanocrystals to Molecules. *Nano Lett.* **2010**, *10*, 318–323.
22. Robel, I.; Kuno, M.; Kamat, P. V. Size-Dependent Electron Injection from Excited CdSe Quantum Dots into TiO_2 Nanoparticles. *J. Am. Chem. Soc.* **2007**, *129*, 4136.
23. Farrow, B.; Kamat, P. V. CdSe Quantum Dot Sensitized Solar Cells. Shuttling Electrons through Stacked Carbon Nanocups. *J. Am. Chem. Soc.* **2009**, *131*, 11124.
24. Huss, A. S.; Bierbaum, A.; Chitta, R.; Ceckanowicz, D. J.; Mann, K. R.; Gladfelter, W. L.; Blank, D. A. Tuning Electron Transfer Rates *via* Systematic Shifts in the Acceptor State Density Using Size-Selected ZnO Colloids. *J. Am. Chem. Soc.* **2010**, *132*, 13963.
25. Tvrdy, K.; Frantsuzov, P. A.; Kamat, P. V. Photoinduced Electron Transfer from Semiconductor Quantum Dots to Metal Oxide Nanoparticles. *Proc. Natl. Acad. Sci. U.S.A.* **2011**, *108*, 29.
26. Zhu, H.; Song, N.; Lian, T. Wave Function Engineering for Ultrafast Charge Separation and Slow Charge Recombination in Type II Core/Shell Quantum Dots. *J. Am. Chem. Soc.* **2011**, *133*, 8762.
27. Ito, Y; Matsuda, K; Kanemitsu, Y. Mechanism of Photoluminescence Enhancement in Single Semiconductor Nanocrystals on Metal Surfaces. *Phys. Rev. B* **2007**, *75*, 033309.
28. Yuan, C. T.; Yu, P.; Tang, J. Blinking Suppression of Colloidal CdSe/ZnS Quantum Dots by Coupling to Silver Nanoprisms. *Appl. Phys. Lett.* **2009**, *94*, 243108.
29. Matsumoto, Y.; Kanemoto, R.; Itoh, T.; Nakanishi, S.; Ishikawa, M.; Biju, V. Photoluminescence Quenching and Intensity Fluctuations of CdSe–ZnS Quantum Dots on an Ag Nanoparticle Film. *J. Phys. Chem. C* **2008**, *112*, 1345–1350.
30. Chen, Z. Y.; Berciaud, S.; Nuckolls, C.; Heinz, T. F.; Brus, L. E. Energy Transfer from Individual Semiconductor Nanocrystals to Graphene. *ACS Nano* **2010**, *4*, 2964–2968.
31. Xu, Z.; Cotlet, M. Quantum Dot–Bridge–Fullerene Heterodimers with Controlled Photoinduced Electron Transfer. *Angew. Chem., Int. Ed.* **2011**, *50*, 6079–6083.
32. Klimov, V. I.; Mikhailovsky, A. A.; McBranch, D. W.; Leatherdale, C. A.; Bawendi, M. G. Quantization of Multiparticle Auger Rates in Semiconductor Quantum Dots. *Science* **2000**, *287*, 1011–1013.
33. Steiner, D.; Dorfs, D.; Banin, U.; Sala, F. D.; Manna, L.; Millo, O. Determination of Band Offsets in Heterostructured Colloidal Nanorods Using Scanning Tunneling Spectroscopy. *Nano Lett.* **2008**, *8*, 2954–2958.
34. Gachet, D.; Avidan, A.; Pinkas, I.; Oron, D. An Upper Bound to Carrier Multiplication Efficiency in Type II Colloidal Quantum Dots. *Nano Lett.* **2010**, *10*, 164–170.

35. Spinicelli, D.; Buil, S.; Quelin, X.; Mahler, B.; Dubertret, B.; Hermier, J. P. Bright and Grey States in CdSe−CdS Nanocrystals Exhibiting Strongly Reduced Blinking. *Phys. Rev. Lett.* **2009**, *102*, 136801–136804.
36. Garcia-Santamaria, F.; Chen, Y. F.; Vela, J.; Schaller, F. D.; Hollingsworth, J. A.; Klimov, V. I. Suppressed Auger Recombination in "Giant" Nanocrystals Boosts Optical Gain Performance. *Nano Lett.* **2009**, *9*, 3482–3488.
37. Sitt, A.; Sala, F. D.; Menagen, G.; Banin, U. Multiexciton Engineering in Seeded Core/Shell Nanorods: Transfer from Type-I to Quasi-Type-II Regimes. *Nano Lett.* **2009**, *9*, 3470–3476.
38. Pisanello, F.; Martiradonna, L.; Lemenager, G.; Spinicelli, P.; Fiore, A.; Manna, L.; Hermier, J. P.; Cingolani, R.; Giacobino, E.; Vittorio, M. D. Room Temperature-Dipolelike Single Photon Source with a Colloidal Dot-in-Rod. *Appl. Phys. Lett.* **2010**, *96*, 033101.
39. Shimoda, H.; Oh, S. J.; Greng, H. Z.; Walker, R. J.; Zhang, X. B.; McNeil, L. E.; Zhou, O. Self-Assembly of Carbon Nanotubes. *Adv. Mater.* **2002**, *14*, 899–901.